A compressive sensing framework for seismic source parameter estimation

Ismael Vera Rodriguez,[1,2] Mauricio Sacchi[1,2] and Yu J. Gu[1]

[1]*Physics Department, University of Alberta, 4-183 CCIS, Edmonton, AB* T6G 2E1*, Canada. E-mail: verarodr@ualberta.ca*
[2]*Signal Analysis and Imaging Group (SAIG), 4-183 CCIS, Edmonton, AB* T6G 2E1*, Canada*

SUMMARY

Simultaneous estimation of origin time, location and moment tensor of seismic events is critical for automatic, continuous, real-time monitoring systems. Recent studies have shown that such systems can be implemented via waveform fitting methods based on pre-computed catalogues of Green's functions. However, limitations exist in the number and length of the recorded traces, and the size of the monitored volume that these methods can handle without compromising real-time response. This study presents numerical tests using a novel waveform fitting method based on compressive sensing, a field of applied mathematics that provides conditions for sampling and recovery of signals that admit a sparse representation under a known base or dictionary. Compressive sensing techniques enable us to determine source parameters in a compressed space, where the dimensions of the variables involved in the inversion are significantly reduced. Results using a hypothetical monitoring network with a dense number of recording stations show that a compressed catalogue of Green's functions with 0.004 per cent of its original size recovers the exact source parameters in more than 50 per cent of the tests. The gains in processing time in this case drop from an estimated 90 days to browse a solution in the uncompressed catalogue to 41.57 s to obtain an estimation using the compressed catalogue. For simultaneous events, the compressive sensing approach does not appear to influence the estimation results beyond the limitations presented by the uncompressed case. The main concern in the use of compressive sensing is detectability issues observed when the amount of compression is beyond a minimum value that is identifiable through numerical experiments. Tests using real data from the 2002 June 18 Caborn Indiana earthquake show that the presence of noise and inaccurate Green's functions require a smaller amount of compression to reproduce the solution obtained with the uncompressed catalogue. In this case, numerical simulation enables the assessment of the amount of compression that provides a reasonable rate of detectability. Overall, the numerical experiments demonstrate the effectiveness of our compressed domain inversion method in the real-time monitoring of seismic sources with dense networks of receivers. As an added benefit of the compression process, the size of the monitored volume can also be increased under specific restrictions while maintaining the real-time response.

Key words: Computational seismology; Early warning; Inverse theory.

GJI Seismology

1 INTRODUCTION

Fast and accurate recovery of seismic source parameters (location, origin time and seismic moment tensor) is a problem of interest in different areas of geophysics. For earthquake monitoring, fast source parameter estimations are routinely conducted at institutions such as the Lamont-Doherty Earth Observatory, where the Global Centroid Moment Tensor project (Dziewonski *et al.* 1981) is presently based, the United States Geological Survey (Sipkin 1982) and the Earthquake Research Institute of Japan (Kawakatsu 1995). Fast inversions are also often performed in the vicinity of

seismically active areas (e.g. Dreger & Helmberger 1993; Pasyanos *et al.* 1996; Dreger 2003; Bernardi *et al.* 2004; Clinton *et al.* 2006; Scognamiglio *et al.* 2009). Furthermore, quick estimations of the source parameters are important for hazard mitigation in mining operations (Trifu & Shumila 2002; Gibowicz 2009), for the evaluation of potential adjustments during/after hydraulic injections in the oil industry (Maxwell *et al.* 2002; LeCampion *et al.* 2004), as well as for monitoring volcanic activities (McNutt 1996; Foulger *et al.* 2004) and fluid injections in geothermal areas (Julian *et al.* 2010). Most inversion algorithms employed in the aforementioned applications do not provide simultaneous estimations of all three source

parameters. Information about origin time and source location is determined by independent systems and/or algorithms, with the source moment tensor being estimated in a secondary step. Therefore, an inherent lag time is required, thus preventing efficient and simultaneous estimation of the three source parameters. Algorithms that do not require a lag time are grid search (Kawakatsu 1998; Tsuruoka *et al.* 2009) and matching pursuit (Vera Rodriguez *et al.* 2012) approaches. Despite their advantages, however, these two methods are also constrained by the maximum numbers of grid nodes and recording stations that can be considered without compromising their real-time response.

Compressive sensing (CS) is a relatively new field of signal processing and applied mathematics that investigates sampling and recovery conditions for signals susceptible to a sparse representation via a known basis or dictionary (Candes *et al.* 2006; Donoho 2006). A major result of CS is the specification of protocols for sampling of signals using a number of non-adaptive measurements that is below the number of samples required with the traditional Nyquist criterion. The non-adaptive measurements are linear combinations of the information contained in the signal weighted by coefficients prescribed in the form of a sensing matrix. In other words, using CS, a signal can be acquired and transmitted in a compressed form, and ultimately uncompressed without perceptive loss of information. This represents an important improvement in efficiency from the traditional practice where a signal is acquired in full form, then compressed throwing away information, transmitted, and finally uncompressed. CS principles have found application in the fields of magnetic resonance imaging (MRI) (Lustig *et al.* 2007), digital camera design (Takhar *et al.* 2006) and acquisition of astronomical data (Bobin *et al.* 2008). In geophysical applications, CS has been implemented for earthquake location (Yao *et al.* 2011), simultaneous estimation of origin time, location and seismic moment tensor (Vera Rodriguez *et al.* 2010), and acquisition of seismic data with simultaneous active sources (Herrmann 2010).

In this study, we introduce the principles of CS into the problem of seismic source parameter estimation. We demonstrate through numerical experiments that the introduction of CS extends the real-time applicability of grid search and matching-pursuit-only methods. Improvements in processing time due to compression enable the monitoring of larger subsurface volumes using significantly denser receiver arrays without compromising real-time response.

2 THEORY AND METHOD

2.1 Parametrization of the source parameter inversion

The forward parametrization of the problem follows that proposed in Vera Rodriguez *et al.* (2012). For brevity, this section mainly reviews the general aspects of this parametrization. Consider a domain of interest for monitoring seismic activity. The region with latent seismicity is enclosed and partitioned using a grid where every grid point is considered a potential or virtual source (Kawakatsu 1998). To record the seismic activity, a network of stations is positioned at arbitrary locations around the monitored volume (Fig. 1). There are no restrictions on the positions of the recording stations, the grid shape and/or the separation between grid nodes. The far-field displacement recorded by a receiver due to a point source at a node of the monitored volume is given by eq. (3.23) in Aki & Richards (2009)

$$\mathbf{u}_n(\mathbf{x}, t) = \mathbf{M}_{pq}(t) * \frac{\partial}{\partial \xi_q} \mathbf{G}_{np}(\mathbf{x}, t; \xi, t_0) , \tag{1}$$
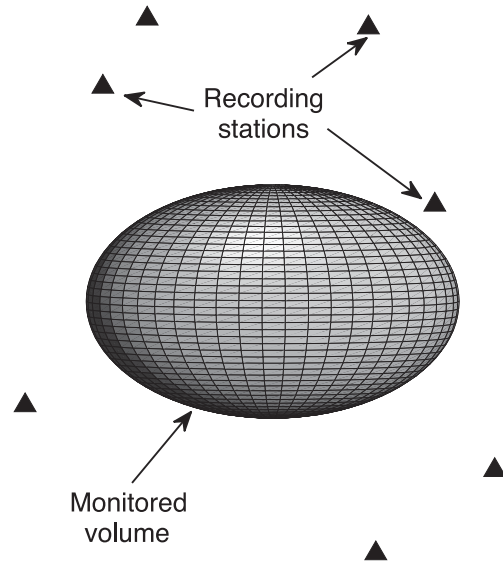

Figure 1. Diagram of the seismic event monitoring setting. The monitored volume (grid) encloses a region with potential seismic activity.

where $\mathbf{x}$ is the location of the recording station and ξ is the location of the seismic source. The term $\mathbf{M}_{pq}(t)$ is the moment tensor of the seismic source with origin time t_0, and $\mathbf{G}_{np}$ are the point source Green's functions containing information about the wave propagation between $\mathbf{x}$ and ξ. The subscript n is related to the station component and the symbol $*$ denotes convolution. Assuming that the source geometry can be separated from its time variation (Madariaga 2007), the seismic moment tensor can be split into a source time function and a scalar moment tensor. Considering the observations from all the stations in the recording network and arranging terms in matrix–vector notation, the displacement field can then be expressed as

$$\mathbf{u} = \mathbf{G}_{(t_0,\xi)} \mathbf{m}_{(t_0,\xi)} . \tag{2}$$

In eq. (2), the column vectors $\mathbf{u}$ and $\mathbf{m}_{(t_0,\xi)}$ contain the observations from all recording stations and the six independent elements of the source moment tensor, respectively. The columns of the matrix $\mathbf{G}_{(t_0,\xi)}$, on the other hand, contain the derivative of the corresponding Green's functions convolved with the source time function. For the rest of the description, it will be of advantage to use the notation

$$\mathbf{G}_{(t_0,\xi)} \mathbf{m}_{(t_0,\xi)} \equiv \mathbf{G}_j[i] \mathbf{m}_j[i] ,$$

where the subindex j is the origin time of the source in number of samples with respect to the first sample of the observations vector $\mathbf{u}$, and the subindex i is manually assigned to the grid node where the source took place. The moment tensors $\mathbf{m}_j[i]$ and the matrices containing Green's functions $\mathbf{G}_j[i]$ will be referred to as blocks and column-blocks, respectively (Eldar *et al.* 2010). If all virtual sources in the monitored volume are considered at once, eq. (2) becomes

$$\mathbf{u} = \sum_{i=1}^{N_{\text{total}}} \mathbf{G}_j[i] \mathbf{m}_j[i] = \mathbf{G}_j \mathbf{m}_j , \tag{3}$$

where the variable N_{total} is the total number of nodes in the grid. Eq. (3) is a sum of the contributions to the displacement field of virtual sources occurring at all grid nodes with the same origin time. The matrix $\mathbf{G}_j$ contains the six Green's functions for all node-station combinations with origin time given by the index j (Fig. 2), whereas
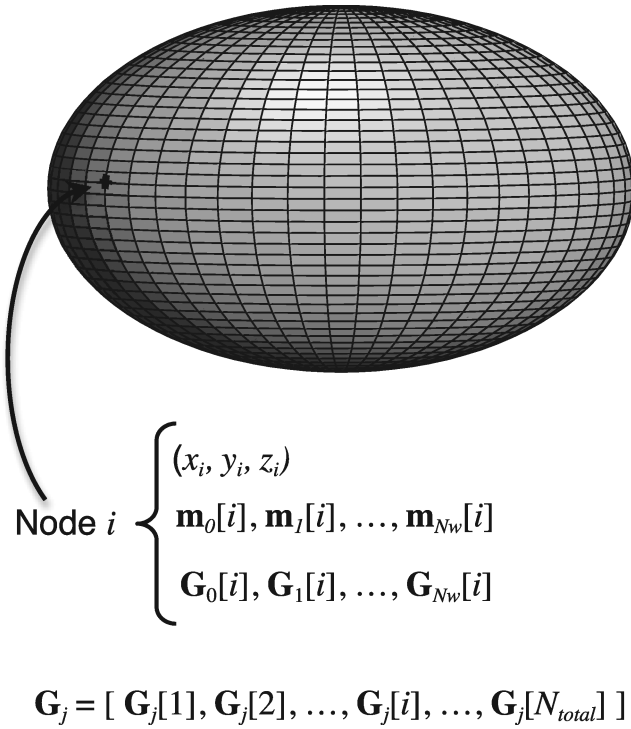
$$\text{Node } i \begin{cases} (x_i, y_i, z_i) \\ \mathbf{m}_0[i], \mathbf{m}_1[i], \ldots, \mathbf{m}_{Nw}[i] \\ \mathbf{G}_0[i], \mathbf{G}_1[i], \ldots, \mathbf{G}_{Nw}[i] \end{cases}$$

$$\mathbf{G}_j = [\ \mathbf{G}_j[1], \mathbf{G}_j[2], \ldots, \mathbf{G}_j[i], \ldots, \mathbf{G}_j[N_{total}]\ ]$$

Figure 2. Construction of a dictionary of Green's functions. The grid nodes are assigned a linear index i, in other words, every index i is related to a position in space (x_i, y_i, z_i). The position index i is also related to virtual sources with origin times specified by a delay index j and moment tensors represented by $\mathbf{m}_j[i]$. The Green's functions that expand the virtual source with moment tensor coefficients $\mathbf{m}_j[i]$ are represented with $\mathbf{G}_j[i]$. A dictionary of Green's functions with origin time given by the index j ($\mathbf{G}_j$) is the concatenation of the sets of six Green's functions of all the nodes in the grid delayed by j samples with respect to the first sample of the observations vector $\mathbf{u}$.

the column vector $\mathbf{m}_j$ includes the moment tensors of all the virtual sources in the grid with origin time j. This formulation can also be extended to consider sources with different origin times in the interval $j \in [0, N_w]$, that is

$$\mathbf{u} = \sum_{j=0}^{N_w} \mathbf{G}_j \mathbf{m}_j = \mathbf{Gm}, \tag{4}$$

where N_w is the length of the processing window. Note that matrix $\mathbf{G}_{j+k}$ is simply a delayed version of matrix $\mathbf{G}_j$ by k samples. In Vera Rodriguez *et al.* (2012), the matrix $\mathbf{G}_j$ is called dictionary, while the matrix $\mathbf{G}$ is referred to as super-dictionary, a term used in that analysis to differentiate $\mathbf{G}_j$ and $\mathbf{G}$. A dictionary $\mathbf{G}_j$ is formed by the concatenation of the column-blocks $\mathbf{G}_j[i], \forall i \in [1, N_{total}]$ (see Fig. 2). Equivalently, a super-dictionary $\mathbf{G}$ is formed either by the set of dictionaries $\mathbf{G}_j$ defined by a single index j (from now on the delay index), or by the set of column-blocks $\mathbf{G}_j[i]$ defined by pairs of indexes (i, j). In a similar way, the vector $\mathbf{m}$ is formed by concatenation of the column vectors $\mathbf{m}_j$ or of the blocks $\mathbf{m}_j[i]$. As an example, the sets of six Green's functions that expand the displacement field of sources located at nodes n_1 and n_2 with origin times t_1 and t_2 are the column-blocks $\mathbf{G}_{(t_1-t_u)/\Delta t}[n_1]$ and $\mathbf{G}_{(t_2-t_u)/\Delta t}[n_2]$, respectively, where t_u is the acquisition time of the first sample in $\mathbf{u}$ and Δt the sampling rate. In such case, the only

virtual sources in $\mathbf{m}$ with moment tensors different from zero would be those given by the blocks $\mathbf{m}_{(t_1-t_u)/\Delta t}[n_1]$ and $\mathbf{m}_{(t_2-t_u)/\Delta t}[n_2]$.

The vector of moment tensors $\mathbf{m}$ is a representation of the displacement field $\mathbf{u}$ under the super-dictionary $\mathbf{G}$. Solving eq. (4) for $\mathbf{m}$ yields the location (index i), origin time (index j) and moment tensor (magnitude of the coefficients in the blocks $\mathbf{m}_j[i]$) of the seismic sources that reproduce the observations vector $\mathbf{u}$. In most seismic monitoring applications of interest, plausible solutions to eq. (4) are block sparse (Eldar *et al.* 2010). In other words, only a small number of blocks $\mathbf{m}_j[i]$ in the solution vector $\mathbf{m}$ contain coefficients that are different from zero. Eq. (4) can be solved in a form that leads to a continuous automatic system; however, immediate limitations for real-time performance are imposed by the number of nodes in the grid, the size of the processing window $[0, N_w]$, and the number and length of the seismic records that enter the system. Augmenting the number of nodes in the grid adds new column-blocks $\mathbf{G}_j[i]$ to each of the dictionaries $\mathbf{G}_j$. Similarly, augmenting the time window $[0, N_w]$ increases the required number of dictionaries $\mathbf{G}_j$. In both cases, the total number of columns of the super-dictionary $\mathbf{G}$ and the length of the solution vector $\mathbf{m}$ are increased. By adding more input records, the observations vector $\mathbf{u}$ and the super-dictionary $\mathbf{G}$ grow in row dimension. The size of the super-dictionary $\mathbf{G}$ has a direct impact on the speed of the algorithms that can be used to solve eq. (4). Seeking sparse solutions presents the advantage that computational speed can increase with the sparsity of the solution. Additionally, computational speed and, for instance, the limits of real-time applicability can also be improved through the use of compressive sensing.

2.2 Compressed domain inversion

As mentioned earlier in Section 1, CS states conditions that permit the signal $\mathbf{u}$ to be recovered from a number of non-adaptive measurements below the minimum number of samples required by the Nyquist criterion. The non-adaptive measurements are random combinations of the samples of the original signal obtained through a sensing matrix $\mathbf{\Phi}$ (Fig. 3), that is,

$$\mathbf{\Phi u} = \mathbf{\Phi GDD}^{-1}\mathbf{m} = \mathbf{\Phi Ab}, \tag{5}$$

where $\mathbf{A} = \mathbf{GD}$ and $\mathbf{b} = \mathbf{D}^{-1}\mathbf{m}$. The variable $\mathbf{D}$ is a diagonal matrix with scalar factors that normalize by energy the columns of $\mathbf{G}$. The energy in $\mathbf{g}_i$, the ith column of matrix $\mathbf{G}$, is given by

$$E_i = \mathbf{g}_i^T \mathbf{g}_i .$$

Hence, the element d_{ii} of $\mathbf{D}$ is given by the square root of the reciprocal of E_i. The sensing matrix $\mathbf{\Phi}$ contains energy-normalized rows and complies with the restricted isometry property (RIP) (Candes *et al.* 2006). Although proving that a matrix complies with the RIP is rather a non-trivial task, it has been showed that matrices with random entries meet with high probability the RIP (Baraniuk *et al.* 2008). Between the most recurred sensing matrix ensembles, it can be counted Gaussian and Bernoulli matrices. In the applications described in this study, Gaussian ensembles are employed. A Gaussian sensing matrix is constructed by drawing random entries from a normal probability density function with zero mean and variance $1/K$ (Baraniuk 2007). The scalar K is the number of measurements left after applying $\mathbf{\Phi}$ and, for instance, is related to the desired amount of compression. Clearly, the random variables that form a sensing matrix are non-adaptive, in other words, the same sensing matrix
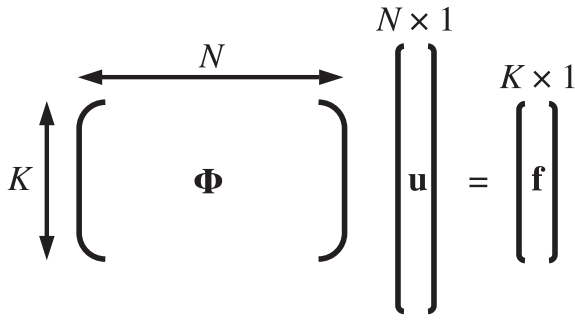
Figure 3. Diagram showing the encoding process of the seismic observations. The sensing matrix $\mathbf{\Phi}$ acts as an encoder compressing the samples in the observations vector $\mathbf{u}$. Assuming that the original signal is sampled at a Nyquist rate, it turns out that the number of non-adaptive measurements that result from encoding $\mathbf{u}$ is less than the number of samples required to sample $\mathbf{u}$ through the Nyquist criterion. CS provides conditions for the encoding and posterior decoding of $\mathbf{f}$ to recover $\mathbf{u}$. Practical CS aims at the development of recording instruments that allow the acquisition of the encoded signal $\mathbf{f}$. In this study, however, CS principles are applied to signals already recorded at a Nyquist rate, where further advantages arise from the processing of those signals in a compressed domain.

can be used for completely different applications. For this reason, the compressed samples are called non-adaptive measurements. The practical effect of the sensing matrix in the system of equations is a dimensionality reduction in the row direction. Consider the dimensions of all the variables in eq. (4): $\mathbf{u} \in \mathbb{R}^{M \times 1}$, where $M =$ number of recording stations $\times$ number of components in each recording station $\times$ number of time samples in each component, $\mathbf{G} \in \mathbb{R}^{M \times N}$, where $N = 6$ (Green's functions) $\times N_{\text{total}}$ (number of nodes in the grid) $\times N_w$ (length of the processing window) and $\mathbf{m} \in \mathbb{R}^{N \times 1}$. Then, by definition, $\mathbf{\Phi} \in \mathbb{R}^{K \times M}$, where $K < M$. Hence, by multiplying eq. (4) times $\mathbf{\Phi}$, the resulting system of equations is 'compressed' from an original domain with dimensions $M \times N$ to a 'compressed domain' with dimensions $K \times N$. The minimum number of non-adaptive measurements K required to recover the original signal $\mathbf{u}$ is related to the sparsity of its representation under $\mathbf{A}$ but not to the original dimensions of $\mathbf{A}$. In the setting of the source monitoring problem, this is a powerful result that indicates the amount of permissible compression is independent of the number of recording stations used for monitoring. As a practical rule of thumb in the noiseless case, more than four non-adaptive measurements per non-zero coefficient in $\mathbf{m}$ (or $\mathbf{b}$) are the minimum required number of samples to recover $\mathbf{u}$ from its compressed version $\mathbf{\Phi}\mathbf{u}$ (Candes & Wakin 2008). CS also imposes the following conditions on the signal $\mathbf{u}$ and the matrix $\mathbf{A}$: (1) $\mathbf{m}$ (or $\mathbf{b}$) is a sparse representation of $\mathbf{u}$ or has non-zero coefficients that decay quickly in absolute magnitude when sorted (i.e. $\mathbf{u}$ is compressible under $\mathbf{A}$); and (2) $\mathbf{\Phi}\mathbf{A}$ also complies with the RIP. The first condition can easily be met since the observations vector $\mathbf{u}$ possesses a sparse representation under

$\mathbf{A}$ for most monitoring scenarios of interest (see previous section). However, the condition related to the product $\mathbf{\Phi}\mathbf{A}$ is not met. The high coherence between the blocks $\mathbf{A}_j[i]$ hinders the recovery of sparse solutions (Vera Rodriguez *et al.* 2012). Given that a practical implementation of the source parameter inversion is far from the settings where the theoretical results of CS can be used to analyse the recovery of optimal solutions, we resort to numerical modelling to assess the applicability of CS in the source parameter inversion problem.

3 NUMERICAL MODELLING

3.1 Seismic monitoring with dense receiver coverage

The first numerical example highlights the advantages of the CS approach in a dense network of recording stations. The monitoring experiment consisting of a network of 441 three-component receivers deployed on the surface to monitor a grid of $45 \times 45 \times 11 = 22\,275$ virtual sources (Fig. 4). The separation between virtual sources is 5 km in the three coordinate directions. Green's functions in real applications should be ideally full waveform traces. In this example, however, we simplify the analysis by using only direct *P*- and *S*-wave arrivals in a homogeneous medium computed with ray tracing theory. Considering the longest arrival time of *S* waves from the ray tracing results and a sampling rate $\Delta t = 0.5$ s, the length of a Green's function for a single component of a receiver is set at 603 samples (301.5 s). To study the impact of the compression on the detectability and accuracy of the source parameters, we select 500 sets of Green's functions with random locations inside the grid and generate synthetic wavefields for each location from a set of six random numbers as the independent elements of the moment tensor. Finally, the synthetic displacements are padded with zeros on both ends to produce observations with duration of 331.5 s with a common origin time at 15 s (this implies a processing window of 30 s or $N_w = 60$). The sensing matrix $\mathbf{\Phi}$ contains independent, identically distributed (i.i.d.) random variables drawn from a Gaussian probability distribution, and five non-adaptive measurements are considered per non-zero coefficient in the expected solution. In other words, assuming that a single source will be represented in each observations vector $\mathbf{u}$, only $K = 30$ samples (six moment tensor coefficients in one source $\times$ five non-adaptive measurements per coefficient) are used to invert for source parameters using the CS approach. If explicitly expressed, the matrix $\mathbf{A}$ with the library of Green's functions should occupy a total memory size of ~ 52 TB. On the other hand, the compressed version of the library of Green's functions ($\mathbf{\Phi}\mathbf{A}$) requires a memory size of ~ 2 GB, and the inversion is solved using a modified version of block orthogonal matching pursuit (BOMP) (Vera Rodriguez *et al.* 2012) that only requires the compressed matrix $\mathbf{\Phi}\mathbf{A}_0$ of ~ 32 MB ($\mathbf{A}_0$ is a version of the dictionary $\mathbf{G}_0$ with columns that are energy-normalized) as input. Hence, with CS, the inversion process becomes easily
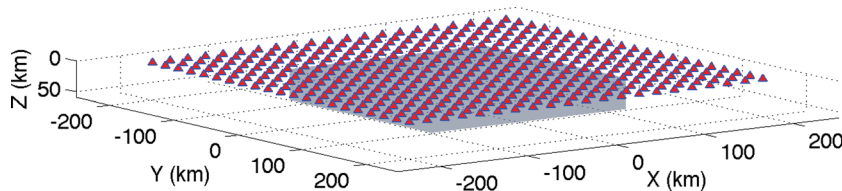

Figure 4. Distribution of recording stations (blue–red triangles) and grid of virtual sources (grey volume) used in the numerical example.
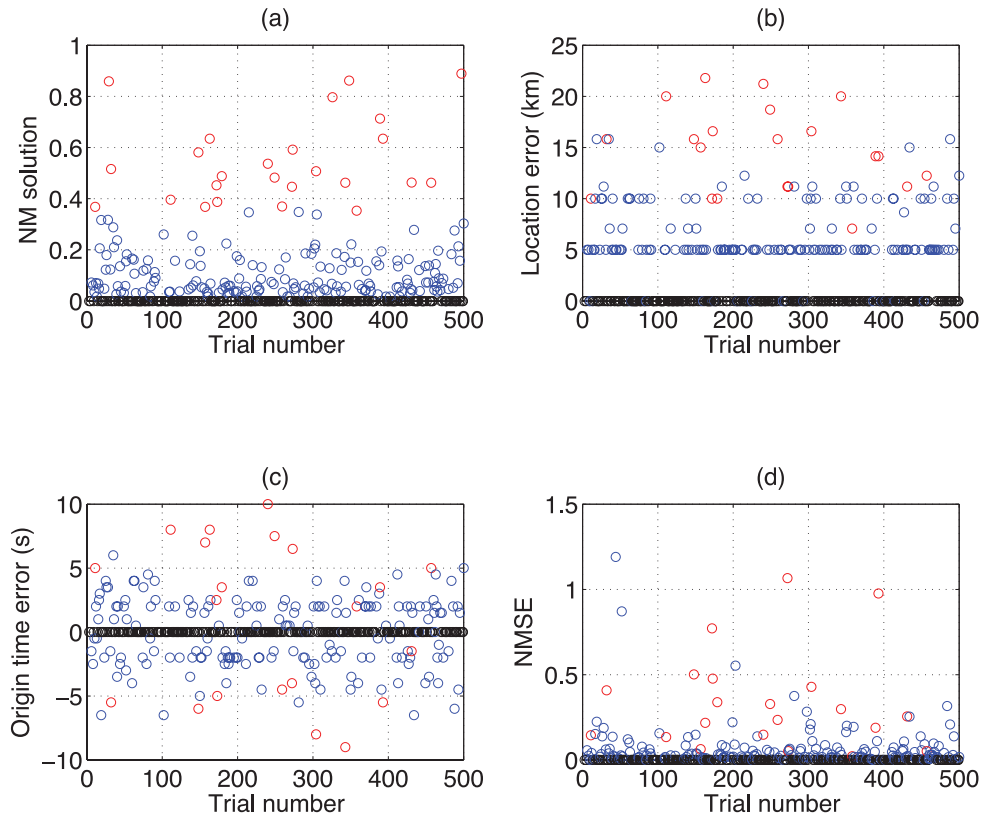
Figure 5. Estimation errors for 500 simulations of source parameter inversion using CS principles. (a) Normalized Misfit of the solution $NM = ||\mathbf{u} - \hat{\mathbf{u}}||_2^2/||\mathbf{u}||_2^2$. (b) Location error $= ||\mathbf{x} - \hat{\mathbf{x}}||_2$, where $\mathbf{x}$ is the true location vector of the source. (c) Origin time error $= OT - \hat{OT}$, where OT is the true origin time. (d) Normalized mean square error of the estimated moment tensor $NMSE = ||\mathbf{m} - \hat{\mathbf{m}}||_2^2/||\mathbf{m}||_2^2$. Variables with a hat denote estimations from the inversion.

tractable using a desktop computer, for example, a four-core desktop computer with 8 GB in RAM and 2.9 GHz processor speed in this study. In this numerical example, we aim to evaluate the efficacy of the inversion method in the source parameter estimation when exact solutions exist, assuming accurate Green's functions and no noise.

The errors in the estimated source parameters for the numerical experiment are presented in Fig. 5. For 500 trials, 51.6 per cent of the sources were detected with no error in the three source parameters, whereas 86.4 per cent had acceptable normalized misfits of 0.35 or below. Finally, 5 per cent of the results showed normalized misfits between 0.35 and 0.8 that, in a practical setting, correspond to undetected sources. In this experiment, 8.6 per cent of the sources had normalized misfits >0.8 (not presented in Fig. 5 due to their large errors). The average processing time to obtain a solution was 41.57 s. In comparison, the estimated time required for the modified BOMP to browse a solution in the full 52 TB library of Green's functions is about 90 days. For the processing window of 30 s, our result can be considered as near real time for the hypothetical monitoring setting. Further improvements to the speed of the inversion algorithm could be achieved by an efficient implementation using parallel processing.

3.2 Simultaneous events

An important benefit of matching pursuit methods when compared to other automatic source parameter inversion algorithms is the possibility to estimate multiple sources embedded in the same observations vector. The second numerical example is aimed to detect the

effect of the inversion method over the estimation of simultaneous events. This objective is addressed by using the same hypothetical monitoring setting of the previous section and the modified BOMP. Two different settings are studied, the first corresponds to two seismic sources with the same source mechanism and location but different origin times. The second scenario consists of the two sources with the same source mechanism and origin time but different locations. For the first case, assume that the seismic sources take place at location n with origin times t_1 and t_2. Setting the acquisition time of the first sample in the observations vector $\mathbf{u}$ to zero, the origin times for the two seismic events in terms of the delay index j are $s_1 = t_1/\Delta t$ and $s_2 = t_2/\Delta t$, respectively. Random numbers are used to simulate a source mechanism for both sources. Using the CS approach, the sources are simultaneously inverted by applying various differences in origin time between them. When the origin time difference is zero, there is technically only one event and the algorithm detects it estimating a moment tensor that is double the size of each individual source (Fig. 6a). As the difference in origin time between the two sources increases, the algorithm's output begins to be affected by the presence of the two displacement fields. For small time differences, the algorithm is unable to resolve the two events. In some cases, the events are not even detected, while biased solutions of the estimated source parameters are given by the algorithm in others. After a certain difference in origin time, the algorithm starts to resolve the presence of the two events; however, we still observe cases where the estimated solutions are biased for one or both events. For the second scenario (Fig. 7), the two seismic sources are inverted while varying the distance between
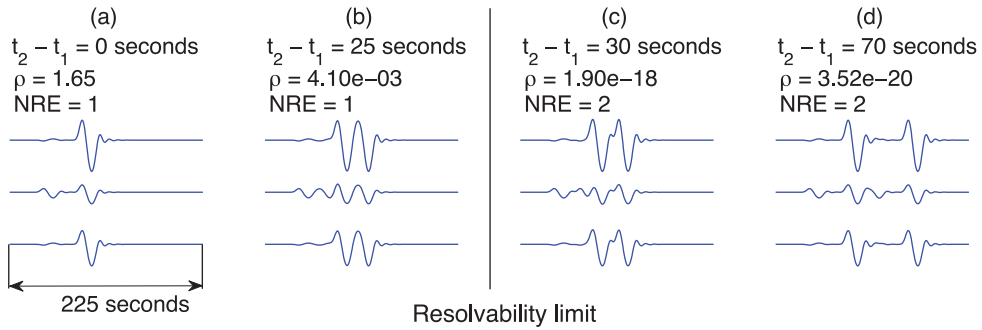
Figure 6. Resolvability of two seismic sources in the same vector of observations. Only observations for one receiver are presented. From top to bottom, the traces correspond to the x (east), y (north) and vertical components of the receiver. NRE is the abbreviation for the number of resolved events by the inversion algorithm. (a) and (b) The algorithm cannot resolve the two sources. (c) and (d) The algorithm is able to resolve the two sources that are also reflected in a sharp decrease in the spectral norm measurement ρ.
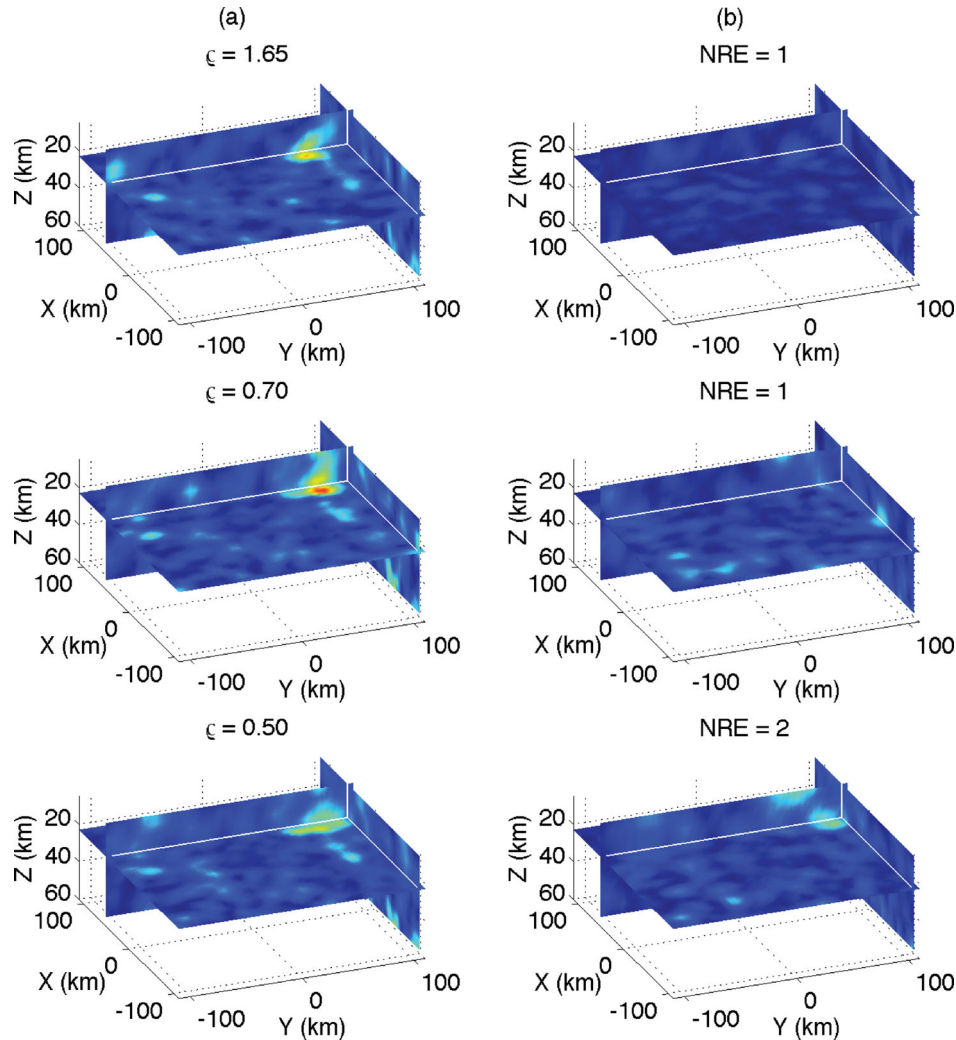
Figure 7. Resolvability of two seismic sources in the same observations vector. The two seismic events have the same origin time and source mechanism. These plots show a snapshot of the objective function used in the modified BOMP at the exact origin time of the sources. (Top) Both sources have the same location. (Middle) Separation between locations is 4 nodes in the y direction (20 km). (Bottom) Separation between locations is 6 nodes in the y direction (30 km). (a) and (b) Columns are, respectively, iterations 1 and 1 of the modified BOMP. Each iteration finds the source parameters of a seismic source. Variable ρ is the spectral norm measurement for each case. NRE stands for number of resolved events.

their locations in the horizontal y direction. In this case, both events have the same origin time and moment tensor. When the locations of the two sources are close, the group sparsity function calculated by the modified BOMP across space and time presents only a single

maximum (Fig. 7a—top and middle plots). After the first iteration, this maximum is extracted and no further sources can be identified (see Fig. 7b—top and middle plots). When the locations of the two sources are far enough, the algorithm is able to determine the

presence of the two seismic events (Fig. 7a—bottom plot). The first event is extracted after the first iteration and the second source is identified as a maximum in the second iteration (Fig. 7b—bottom plot). One way to identify the resolvability limit where the algorithm begins to resolve the two events is by analysing the measure

$$\rho\left((\mathbf{G}_{s_1}[n])^T \mathbf{G}_{s_2}[n]\right),$$

where $\rho(\cdot)$ is the spectral norm operator (Strang 2006). As the spectral norm measurement reduces, the algorithm is able to resolve the presence of the two events. In the case of the events with different origin time, the limit of resolvability is particularly evident as a sharp drop in the spectral norm measurement (see Fig. 6); this might also partly result from the simplicity of the Green's functions used in this example. In both multiple source experiments, we identify detectability issues that seemed unrelated to the resolvability of the algorithm. The detectability of the algorithm is mainly influenced by the coherence of the dictionary of Green's functions. The high coherence nature of the dictionary is expressed in the presence of multiple local maxima in the objective function (correlation between compressed Green's functions and residuals) calculated by the modified BOMP (see Fig. 7). The modified BOMP partially improves detectability by re-visiting a number of maxima in the objective function. The objective of re-visiting only a subset of maxima values is to reduce computational time; however, this is at the cost of potentially missing observed seismic events. In the limit when the modified BOMP re-visits the whole objective function, this becomes equivalent to a standard grid search method. Resolvability and detectability considerations in these numerical examples arise from the combined use of sparse representation theory with CS. The following example using real earthquake data isolates the effect of the compression process on the detectability of seismic events.

3.3 Earthquake monitoring

The final example explores the influence of different compression rates and realizations of sensing matrices into the inversion results. This example utilizes data from an earthquake that occurred on 2002 June 18 in Caborn Indiana. The Caborn event is a moderate-sized earthquake ($M_w = 4.6$) that took place within the limits of the Wabash Valley Fault System (WVFS) (Fig. 8). The WVFS is a part of the Wabash Valley Seismic Zone (WVSZ) located in the central eastern area of the United States (Langer & Bollinger 1991). The WVFS is a system of high-angle subsurface normal faults that run parallel to the Wabash River Valley. The source parameters of this earthquake have been previously estimated in an earlier analysis using a combination of inversion methods (Fig. 8, Table 1), and also with a hypothetical real-time monitoring system based on a sparse representation (Table 1). Based on an analysis that included the 2002 June 18 Caborn earthquake, Kim (2003) interpreted the reactivation of a possible Precambrian rift system by the contemporary regional stresses. The objective of computing the source parameters of the Caborn earthquake in this study is not to obtain new or refined estimates of already accepted values, but to test if the CS approach can reproduce previous estimations. In the best case scenario, the CS approach should reproduce the results obtained with the uncompressed dictionary with the advantage of improved processing speed.

For comparison purposes, we test the CS approach using the same hypothetical monitoring system described in Vera Rodriguez *et al.* (2012). The system continuously inverts the recordings of eight
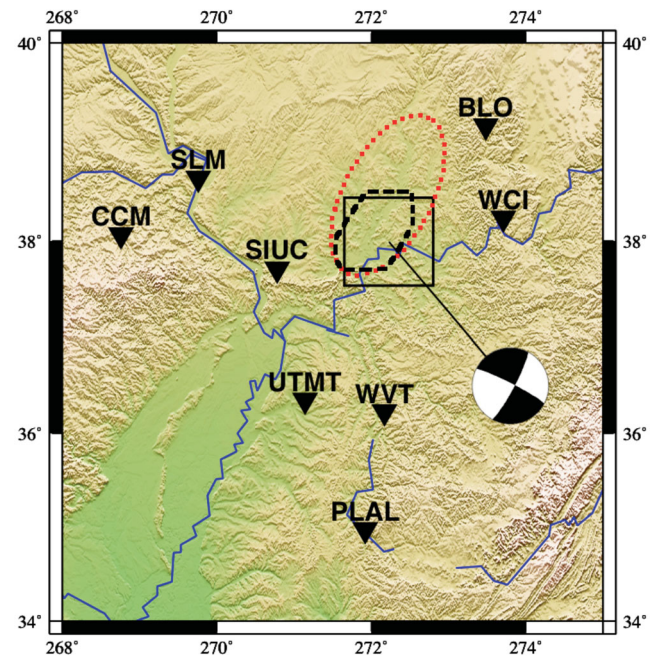
Figure 8. Distribution of recording stations considered in the inversion tests for the 2002 June 18 Caborn earthquake (black triangles). The black square represents the surface projection of the monitoring grid. The dotted line delimits the WVSZ, and the dashed line the WVFS. The beach ball representation corresponds to the solution determined by Kim (2003) joined by a line to its epicentral location. Image after Vera Rodriguez *et al.* (2012).

broadband seismic stations located within 300 km from WVFS (see Fig. 8). The monitored volume comprises 2205 virtual sources arranged in a regular grid of $21 \times 21 \times 5$ nodes with separations of 5 km in the three coordinate directions. Both Green's functions and observations are rotated to a radial, transverse and vertical system, and the velocity seismograms are band-limited to the frequency range of 0.01–0.1 Hz. Green's functions are calculated with the reflectivity method of Randall (1994) using a three-layer velocity model with compressional velocities: 5.9, 6.5 and 8.0 km s^{-1}, shear velocities: 3.4, 3.7 and 4.5 km s^{-1}, and layer interface depths: 7 and 28 km (Kim 2003). The duration of a Green's function is 150 s that also corresponds to 150 samples given the sampling rate of 1 s in the seismic traces. The processing window is $N_w = 30$ samples; hence, the total length of a vector of observations $\mathbf{u}$ is 180 samples. To simulate the continuous monitoring of seismic activity, a time window of $[-60, 240]$ s is selected relative to the origin time (Kim 2003). The inversion is solved using the modified BOMP methodology with the same parameters employed in Vera Rodriguez *et al.* (2012) that include (1) a deviatoric constraint and (2) re-visiting the 200 highest local maxima of the objective function in the modified BOMP to look for optimal solutions. The monitoring simulation is performed six times with different degrees of compression corresponding to 5, 10, 20, 30, 40 and 120 non-adaptive samples per non-zero coefficient (NNA) in the solution vector $\mathbf{m}$. In each simulation, 500 realizations of sensing matrix are examined, where each matrix is generated by drawing i.i.d. random variables from a Gaussian probability distribution. The CS approach recovers successfully the source parameters of the Caborn earthquake within a negligible variation margin (Table 1). The parameter with a slightly larger variation is the depth, though the CS results still fall between the depth of 18 km determined by Kim (2003) and 20.5 km by Vera Rodriguez *et al.* (2012). The main

Table 1. Comparison of different solutions for the June 18, Caborn earthquake. NNA stands for the number of non-adaptive measurements per non-zero coefficient in the CS solution. DS stands for dictionary size after compression, where 100 per cent corresponds to the uncompressed dictionary. Success rate refers to the percentage of times that the event was detected using the CS approach in 500 realizations of sensing matrix.

Solution	Success rate (per cent)	Origin time 17 hr 37 min + (s)	Location	Source mechanism
Kim (2003)	N/A	17.2	37.99° N 87.77° W Depth (18 ± 2) km	
Vera Rodriguez *et al.* (2012)	N/A	16.0	37.988° N 87.770° W Depth 20.5 km	
CS NNA = 5 DS = 0.7 per cent	4.6	16.0 ± 0.2	(37.988 ± 0.000)° N (87.770 ± 0.000)° W Depth (18.98 ± 2.35) km	
NNA = 20 DS = 2.8 per cent	31.4	16.0 ± 0.0	(37.988 ± 0.000)° N (87.770 ± 0.000)° W Depth (20.21 ± 1.17) km	
NNA = 40 DS = 5.6 per cent	60.0	16.0 ± 0.0	(37.988 ± 0.000)° N (87.770 ± 0.000)° W Depth (20.47 ± 0.41) km	
NNA = 120 DS = 16.7 per cent	96.8	16.0 ± 0.0	(37.988 ± 0.000)° N (87.770 ± 0.000)° W Depth (20.50 ± 0.00) km	

concern in the application of CS is detectability. The success rate for low NNA is around 4.6 per cent. This small value contrasts with the 86.4 per cent observed in the first synthetic experiment using the same amount of compression. The difference in success rate suggests an important impact in detectability due to the use of inaccurate Green's functions and the presence of noise in the real data. Reducing the amount of compression offsets the negative effect in detectability. For instance, a reasonable success rate of 96.8 per cent is observed for NNA = 120, which corresponds to a compression of 16.7 per cent relative to the uncompressed dictionary size of 100 per cent. More remarkably, at this compression level, the CS approach reproduced the source parameters for all the realizations of sensing matrix where the earthquake was detected. In other words, no effect of the compression process was visible from the results. As the NNA increases, the CS results tend to converge towards the source parameters obtained without CS (Fig. 9a). The faster the CS results converge the more advantageous the CS approach becomes since smaller dictionaries are needed to perform the inversion. For the source parameters, the convergence also implies that the results are unaffected by the choice of sensing matrix used for compression. In the case of the modified BOMP performance, the increase in the NNA also reduces the size of the search for optimal solutions (Fig. 9b), which compensates the increase in processing time due to a lower compression rate. The gains in processing time with CS in this example are rather moderate (Fig. 9c), because the absolute size of the compressed dictionaries does not represent a substantial difference for the computer capabilities (the uncompressed dictionary size is ~350 MB). The CS approach is feasible in the hypothetical Caborn monitoring system and enables a large number of monitoring stations to be inverted in real time. The benefits for real-time monitoring provided by CS would be more apparent as the number of recording stations in the monitoring system increases.

4 DISCUSSION

The implementation of grid search approaches in different areas of science and engineering has became possible with the development of more powerful and less expensive computing systems. In the case of seismic source monitoring, the grid search approach still requires a considerable amount of computing resources to handle large quantities of seismic records in a dense monitoring grid. As a reference, Tajima *et al.* (2002) evaluate the feasibility of the grid search approach using real data from the Berkeley Digital Seismic Network. Considering the computational resources available for their analysis, the authors estimated a total of 12 min for the processing of the records from three broadband seismic stations in a grid with 160 virtual sources using a processing window of 20 s. They also acknowledged that the task of reading Green's functions from hard disk occupies a significant amount of the processing time, suggesting parallel processing in a cluster of workstations as an alternative to achieve the real-time response of the system. Tsuruoka *et al.* (2009) present the results of implementation of the grid search monitoring approach in Japan. In this case, real-time response was achieved in a monitoring grid consisting of 6875 virtual sources using three seismic stations. The authors further suggest that improvements in computer performance would allow the monitoring of more than 7000 virtual sources using also a larger number of seismic stations. The sparse representation inversion presented in Vera Rodriguez *et al.* (2012) performs with an ample margin the real-time inversion of the Caborn, Indiana, earthquake using 2205 virtual sources with the records from eight broadband seismic stations. Although less virtual sources are employed in this latter study, the use of more seismic stations puts this result in a comparable setting to those of the previous grid search experiments. In contrast to these results, the compressed domain inversion presented in this
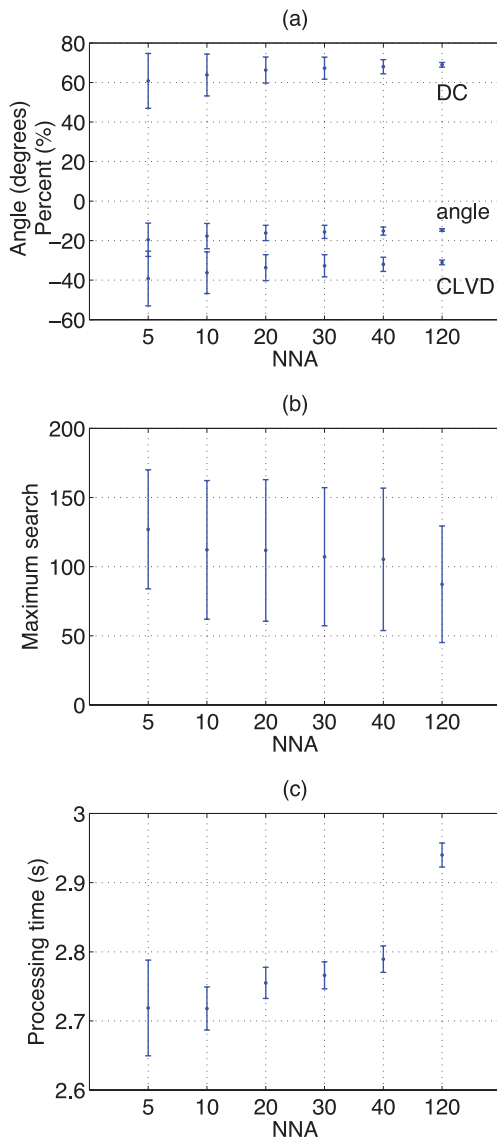
Figure 9. Results for 500 realizations of sensing matrix in five different scenarios of compression to detect and estimate source parameters for the 2002 June 18 Caborn earthquake. NNA stands for number of non-adaptive measurements per non-zero coefficient in the solution. Vertical bars are standard deviations. (a) Average source decompositions, *y*-axis is percentage for DC and CLVD components (Knopoff & Randall 1970), and degrees for the angle between the slip vector and the fault plane (Vavrycuk 2001). (b) Average position of the value in the correlation function between compressed Green's functions and residuals in BOMP where the solution was found. (c) Average processing time.

study can perform in real time using the same computational resources for a considerably larger amount of seismic records. Also, the reduction in variable size permits the use of denser monitoring grids as illustrated in the first synthetic example of this study, where a grid of 22 275 virtual sources is inverted for the case of 441 receivers. Simultaneous source parameter estimation approaches are an attempt to improve the response time of monitoring systems based on the two-step estimation procedure. For example, Tajima *et al.* (2002) presents the grid search approach as an alternative to the two-step system deployed in the Berkeley Seismological Laboratory, which relied from information about origin time and source location produced by the United States Geological Survey.

Transmission of information about origin time and location from one place to another directly impacts the response time to provide estimations that include the moment tensor of the seismic event. Table 2 presents a comparison between the general steps involved in the source parameter determination followed by the two step and the simultaneous approaches. In the best case scenario, the response time when the two-step approach is performed automatically by the same computer can be similar or better to the simultaneous approaches. However, even in this case, the source parameters obtained by the simultaneous algorithms are the best overall, while the two-step solutions present unrelated estimation errors. A larger amount of recordings can potentially be used in real time if the moment tensor inversion method employed in the two-step procedure does not require full waveform information. Nevertheless, the maximum number of recordings will always be limited at some point by the computational resources. The compressed domain inversion is, on the other hand, not directly limited by computational resources, as the maximum amount of compression does not depend on the number of input records but on the number of expected seismic sources in the solution. A major advantage in the two-step procedure is its flexibility, for instance, more accurate solutions can be obtained by manually manipulating and validating the results at each step. In the case of the simultaneous approaches, the use of fixed grids impacts the accuracy of the source locations by design, while there is no room for manual tuning of the intermediate inversion stages. Flexibility and accuracy are somehow sacrificed in favour of faster estimations in the simultaneous approaches. If the purpose of the system is real-time response, the trade-off between accuracy and speed is unavoidable, nevertheless simultaneous approaches are specifically developed to handle efficiently this juncture.

5 CONCLUSIONS

Real-time simultaneous estimation of the source parameters has applications in different areas of geophysics. This study presents a new method for the automatic recovery of source parameters based on ideas of compressive sensing. The main advantage of our method is that a large number of recordings can be inverted without compromising real-time response. Furthermore, if the compression rate is correctly selected, the results obtained by the compressed domain methodology would be identical to those without using compression, with the added benefit of a shorter processing time. The application of compressive sensing does require a dictionary of Green's functions that embodies the properties of a low-coherency frame. Moreover, the lack of practical dictionaries that meet this assumption necessitates the use of numerical modelling as a vital tool to determine the feasibility of applying the compressive sensing approach in a given scenario. A complete implementation of compressive sensing to the source monitoring problem requires the setting of new acquisition protocols that allow the recording of the compressed measurements. Even in the absence of such protocols, a proper use of compressive sensing can be an effective tool for real-time monitoring of seismic events.

Table 2. Comparison of the general steps involved in the estimation of the source parameters between the two-step versus the simultaneous approach. Advantages and disadvantages are considered in terms of the speed to generate results and their reliability.

STEP	Two-step approach		Simultaneous approach	
	Advantages	Disadvantages	Advantages	Disadvantages
Feeding of data	Assuming continuous feeding of records from the seismic stations to the computing centre in both cases			
Origin time and location estimation	Faster when only first breaks are required			Full waveform information needs to be available to start computations
Transmission	Depends on the location of the system that performs the source mechanism inversion. Best case: the source mechanism inversion is performed by the same computer. Worst case: origin time and location are received from a system in a different geographical location.		No further transmission of data required	
Start moment tensor estimation		Only after information about location and origin time is received.	Continuous monitoring for the three source parameters in all available data	
Data preparation	Depends if the procedure is automatic, semiautomatic or manual, and the type of moment tensor inversion. Best case: automatic system with moment tensor inversion that does not require full waveform information. Worst case: manual system with a moment tensor inversion that requires full waveform information.		No further data preparation required	
Moment tensor inversion with full waveform method	More information per record to constraint the inversion	More sensitive to inaccurate velocity model. Limited number of records that can be inverted in real-time.	More information per record to constraint the inversion. Compressed domain inversion extends the real-time limits.	More sensitive to inaccurate velocity model. Detectability considerations in the compressed domain inversion.
Moment tensor inversion with method that does not require full waveform information.	Faster results	Less information per record to constraint inversion (less robust than full waveform)		
Refinement of source parameters		Refinements are possible but require to re-initialize the two-step procedure.	The first output is the best approximation achievable by the system. No refinement is required.	
Accuracy of results	More accurate if there is manual validation and refinement but more time-consuming.	Source parameters are only optimal for the individual algorithms that obtained them, but not as a group. Other potential issues depend on the specific inversion methodologies.	Subjected to spatial and temporal sampling and accuracy of Green's functions. Detectability considerations in compressed inversion. Advantage: the three source parameters are optimal as a group. Disadvantage: noisy records cannot be discarded.	

REFERENCES

Aki, K. & Richards, P., 2009. *Quantitative Seismology,* University Science Books, Sausalito, CA.

Baraniuk, R., 2007. Compressive sensing, *IEEE Signal Process. Mag.,* **24,** 118–121.

Baraniuk, R., Davenport, M., DeVore, R. & Wakin, M., 2008. A simple proof of the restricted isometry property for random matrices, *Constr. Approx.,* **28**(3), 253–263.

Bernardi, F., Braunmiller, J., Kradolfer, U. & Giardini, D., 2004. Automatic regional moment tensor inversion in the European-mediterranean region, *Geophys. J. Int.,* **157**(2), 703–716.

Bobin, J., Starck, J. & Ottensamer, R., 2008. Compressed sensing in astronomy, *IEEE J. Sel. Topics Signal Process.,* **2,** 718–726.

Candes, E., Romberg, J. & Tao, T., 2006. Robust uncertainty principles: exact signal reconstruction from highly incomplete frequency information, *IEEE Trans. Inf. Theory,* **52,** 489–509.

Candes, E. & Wakin, M., 2008. An introduction to compressive sampling, *IEEE Signal Process. Mag.,* **25,** 21–30.

Clinton, J., Hauksson, E. & Solanki, K., 2006. An evaluation of the scsn moment tensor solutions: robustness of the m_W magnitude scale, style of faulting and automation of the method, *Bull. seism. Soc. Am.,* **96,** 1689–1705.

Donoho, D., 2006. Compressed sensing, *IEEE Trans. Inf. Theory,* **52,** 1289–1306.

Dreger, D., 2003. Tdmt_inv: Time domain seismic moment tensor inversion, in *International Handbook of Earthquake and Engineering Seismology,* Int. Geophys., Vol. 81B, pp. 1627–1627, eds Lee, W., Kanamori, H., Jennings, P. & Kisslinger, C., Academic Press, San Diego, CA.

Dreger, D. & Helmberger, D., 1993. Determination of source parameters at regional distances with single station or sparse network data, *J. geophys. Res.,* **98,** 8107–8125.

Dziewonski, A., Chou, T. & Woodhouse, J., 1981. Determination of earthquake source parameters from waveform data for studies of global and regional seismicity, *J. geophys. Res.,* **86,** 2825–2852.

Eldar, Y.C., Kuppinger, P. & Bolcskei, H., 2010. Block-sparse signals: uncertainty relations and efficient recovery, *IEEE Trans. Signal Process.,* **58**(6), 3042–3054.

Foulger, G., Julian, B., Hill, D., Pitt, A., Malin, P. & Shalev, E., 2004. Non-double-couple microearthquakes at Long Valley Caldera, California, provide evidence for hydraulic fracturing, *J. Volc. Geotherm. Res.,* **132,** 45–71.

Gibowicz, S., 2009. *Seismicity Induced by Mining: Recent Research,* Adv. Geophys., Vol. 51, pp. 1–53, ed. Dmowska, R., Elsevier, Amsterdam.

Herrmann, F., 2010. Randomized sampling and sparsity: getting more information from fewer samples, *Geophysics,* **75,** WB173–WB187.

Julian, B., Foulger, G., Monastero, F. & Bjornstad, S., 2010. Imaging hydraulic fractures in a geothermal reservoir, *Geophys. Res. Lett.,* **37,** L07305, doi:10.1029/2009GL040933.

Kawakatsu, H., 1995. Automated near-realtime cmt inversions, *Geophys. Res. Lett.,* **94,** 2569–2572.

Kawakatsu, H., 1998. On the realtime monitoring of the long-period seismic wavefield, *Bull. Earthq. Res. Inst.,* **73,** 267–274.

Kim, W., 2003. The 18 June 2002 Caborn, Indiana, earthquake: reactivation of ancient rift in the Wabash Valley seismic zone?, *Bull. seism. Soc. Am.,* **93,** 2201–2211.

Knopoff, L. & Randall, M., 1970. The compensated linear-vector dipole: a possible mechanism for deep earthquakes, *J. geophys. Res.,* **75,** 4957–4963.

Langer, C. & Bollinger, G., 1991. The Southeastern Illinois earthquake of 10 June 1987: the later aftershocks, *Bull. seism. Soc. Am.,* **81,** 423–445.

LeCampion, B., Jeffrey, R. & Detournay, E., 2004. Real-time estimation of fracture volume and hydraulic fracturing treatment efficiency, in *Proceedings of the 6th North America Rock Mechanics Symp.,* Paper ID 04-519, 9 p., American Rock Mechanics Association, Houston, TX.

Lustig, M., Donoho, D. & Pauly, J., 2007. Sparse mri: the application of compressed sensing for rapid mr imaging, *Magn. Reson. Med.,* **58,** 1182–1195.

Madariaga, R., 2007. Seismic source theory, in *Treatise on Geophysics,* pp. 59–82, ed. Schubert, G., Elsevier, Amsterdam.

Maxwell, S., Urbancic, T., Steinsberger, N. & Zinno, R., 2002. Microseismic imaging of hydraulic fracture complexity in the Barnett shale, in *Proceedings of SPE Annual Technical Conference and Exhibition,* Paper SPE77440, San Antonio, TX.

McNutt, S., 1996. Seismic monitoring and eruption forecasting of volcanoes: a review of the state-of-the-art and case histories, in *Monitoring and Mitigation of Volcano Hazards,* pp. 99–146, eds Scarpa, R. & Tilling, R., Springer-Verlag, Berlin.

Pasyanos, M., Dreger, D. & Romanowicz, B., 1996. Toward real-time estimation of regional moment tensors, *Bull. seism. Soc. Am.,* **86,** 1255–1269.

Randall, G., 1994. Efficient calculation of complete differential seismograms for laterally homogeneous Earth models, *Geophys. J. Int.,* **118,** 245–254.

Scognamiglio, L., Tinti, E. & Michelini, A., 2009. Real-time determination of seismic moment tensor for the Italian region, *Bull. seism. Soc. Am.,* **99,** 2223–2242.

Sipkin, S.A., 1982. Estimation of earthquake source parameters by the inversion of waveform data: synthetic waveforms, *Phys. Earth planet. Inter.,* **30**(2-3), 242–259.

Strang, G., 2006. *Linear Algebra and Its Applications,* Thomson Brooks/Cole, Toronto.

Tajima, F., Megnin, C., Dreger, D. & Romanowicz, B., 2002. Feasibility of real-time broadband waveform inversion for simultaneous moment tensor and centroid location determination, *Bull. seism. Soc. Am.,* **92,** 739–750.

Takhar, D., Laska, J., Wakin, M., Duarte, M., Baron, D., Sarvotham, S., Kelly, K. & Baraniuk, R., 2006. A new compressive imaging camera architecture using optical-domain compression, in *Proceedings of Computational Imaging IV,* San Jose, CA, pp. 43–52.

Trifu, C. & Shumila, V., 2002. Reliability of seismic moment tensor inversions for induced microseismicity at Kidd Mine, Ontario, *Pure appl. Geophys.,* **159,** 145–164.

Tsuruoka, H., Kawakatsu, H. & Urabe, T., 2009. Grid mt (grid-based real-time determination of moment tensors) monitoring the long-period seismic wavefield., *Phys. Earth planet. Inter.,* **175,** 8–16.

Vavrycuk, V., 2001. Inversion for parameters of tensile earthquakes, *J. geophys. Res.,* **106,** 16 339–16 355.

Vera Rodriguez, I., Sacchi, M. & Gu, Y., 2010. Towards a near real-time system for event hypocenter and source mechanism recovery via compressive sensing, *SEG Expanded Abstr.,* **29,** 2140–2145.

Vera Rodriguez, I., Sacchi, M. & Gu, Y., 2012. Simultaneous recovery of origin time, hypocentre location and seismic moment tensor using sparse representation theory, *Geophys. J. Int.,* **188,** 1188–1202.

Yao, H., Gerstoft, P., Shearer, P. & Mecklenbrauker, C., 2011. Compressive sensing of the Tohoku-Oki mw 9.0 earthquake: frequency-dependent rupture modes, *Geophys. Res. Lett.,* **38,** L20310, doi:10.1029/2011GL049223.